JAMA | Original Investigation

Neuroimaging Findings in US Government Personnel With Possible Exposure to Directional Phenomena in Havana, Cuba

Ragini Verma, PhD; Randel L. Swanson, DO, PhD; Drew Parker, BS; Abdol Aziz Ould Ismail, MD; Russell T. Shinohara, PhD; Jacob A. Alappatt, BTech; Jimit Doshi, MS; Christos Davatzikos, PhD; Michael Gallaway, OD; Diana Duda, PT, DPT; H. Isaac Chen, MD; Junghoon J. Kim, PhD; Ruben C. Gur, PhD; Ronald L. Wolf, MD, PhD; M. Sean Grady, MD; Stephen Hampton, MD; Ramon Diaz-Arrastia, MD, PhD; Douglas H. Smith, MD

IMPORTANCE United States government personnel experienced potential exposures to uncharacterized directional phenomena while serving in Havana, Cuba, from late 2016 through May 2018. The underlying neuroanatomical findings have not been described.

OBJECTIVE To examine potential differences in brain tissue volume, microstructure, and functional connectivity in government personnel compared with individuals not exposed to directional phenomena.

DESIGN, SETTING, AND PARTICIPANTS Forty government personnel (patients) who were potentially exposed and experienced neurological symptoms underwent evaluation at a US academic medical center from August 21, 2017, to June 8, 2018, including advanced structural and functional magnetic resonance imaging analytics. Findings were compared with imaging findings of 48 demographically similar healthy controls.

EXPOSURES Potential exposure to uncharacterized directional phenomena of unknown etiology, manifesting as pressure, vibration, or sound.

MAIN OUTCOMES AND MEASURES Potential imaging-based differences between patients and controls with regard to (1) white matter and gray matter total and regional brain volumes, (2) cerebellar tissue microstructure metrics (eg, mean diffusivity), and (3) functional connectivity in the visuospatial, auditory, and executive control subnetworks.

RESULTS Imaging studies were completed for 40 patients (mean age, 40.4 years; 23 [57.5%] men; imaging performed a median of 188 [range, 4-403] days after initial exposure) and 48 controls (mean age, 37.6 years; 33 [68.8%] men). Mean whole brain white matter volume was significantly smaller in patients compared with controls (patients: 542.22 cm^3; controls: 569.61 cm^3; difference, −27.39 [95% CI, −37.93 to −16.84] cm^3; P < .001), with no significant difference in the whole brain gray matter volume (patients: 698.55 cm^3; controls: 691.83 cm^3; difference, 6.72 [95% CI, −4.83 to 18.27] cm^3; P = .25). Among patients compared with controls, there were significantly greater ventral diencephalon and cerebellar gray matter volumes and significantly smaller frontal, occipital, and parietal lobe white matter volumes; significantly lower mean diffusivity in the inferior vermis of the cerebellum (patients: 7.71 × 10^{-4} mm^2/s; controls: 8.98 × 10^{-4} mm^2/s; difference, −1.27 × 10^{-4} [95% CI, −1.93 × 10^{-4} to −6.17 × 10^{-5}] mm^2/s; P < .001); and significantly lower mean functional connectivity in the auditory subnetwork (patients: 0.45; controls: 0.61; difference, −0.16 [95% CI, −0.26 to −0.05]; P = .003) and visuospatial subnetwork (patients: 0.30; controls: 0.40; difference, −0.10 [95% CI, −0.16 to −0.04]; P = .002) but not in the executive control subnetwork (patients: 0.24; controls: 0.25; difference: −0.016 [95% CI, −0.04 to 0.01]; P = .23).

CONCLUSIONS AND RELEVANCE Among US government personnel in Havana, Cuba, with potential exposure to directional phenomena, compared with healthy controls, advanced brain magnetic resonance imaging revealed significant differences in whole brain white matter volume, regional gray and white matter volumes, cerebellar tissue microstructural integrity, and functional connectivity in the auditory and visuospatial subnetworks but not in the executive control subnetwork. The clinical importance of these differences is uncertain and may require further study.

JAMA. 2019;322(4):336-347. doi:10.1001/jama.2019.9269

+ Supplemental content

Several US government personnel serving in Havana, Cuba, reported potential directional phenomena exposure between late 2016 and May 2018[1] and underwent clinical evaluation and treatment at the University of Pennsylvania's (Penn's) Center for Brain Injury and Repair. This cohort (hereafter referred to as patients) was found to have a heterogeneous combination of nonspecific neurological manifestations including oculomotor, vestibular, and cognitive findings that, when persistent, required comprehensive outpatient neurological rehabilitation.[2] As reported previously,[2] clinical neuroradiological evaluation focused primarily on review of conventional fluid-attenuated inversion recovery (FLAIR) and T1- and T2-weighted magnetic resonance imaging (MRI) acquisitions did not identify an underlying neuroanatomic basis for the observed clinical manifestations in the patients.

As part of the investigation into the patients' signs and symptoms, advanced neuroimaging was conducted with multimodal MRI, including conventional 3D FLAIR, T1- and T2-weighted, and more advanced diffusion MRI (dMRI) (both diffusion tensor imaging [DTI] and its higher angular counterpart)[3,4] and resting-state functional MRI (rs-fMRI). The multimodal imaging-based investigation was undertaken to examine potential differences in brain volume, tissue microstructural integrity, and functional connectivity (each with their own hypotheses) between the patients who had reported potential directional phenomena exposure while serving in Havana, Cuba, and demographically similar healthy controls. In brain volume analysis, the hypothesis was that there would be a difference in overall white and gray matter volume between patients and controls as well as volume differences in anatomical structures. In the analysis of tissue microstructural integrity, the primary hypothesis was that there would be differences in the cerebellum between patients and controls, and the secondary hypothesis was that there would be differences in the cerebrum. In analysis of functional connectivity, the hypothesis was that there would be a difference between the auditory, visuospatial, or executive control subnetworks of patients compared with controls.

Methods

Participants and Study Design

The US Department of State directly referred personnel and family members to the University of Pennsylvania[1] for clinical evaluation and treatment following potential exposure to directional phenomena while serving in Havana, Cuba, between late 2016 and May 2018. Neurological findings among 21 of these patients were previously described in a preliminary clinical report[2] (eTables 1 and 2 in the Supplement).

The advanced neuroimaging analysis reported in this retrospective study was approved by the institutional review board of the University of Pennsylvania. Written or oral informed consent was obtained from all patients except 4 who were unreachable. The institutional review board waived the need to obtain consent from these 4 people prior to including their imaging data in the analysis because they were unreachable by any mode of communication. Written consent was obtained for controls. Advanced neuroimaging was performed to aid in the clinical evaluation of potential brain injury using an MRI acquisition protocol similar to a standard extended brain injury MRI protocol. For this report, patients with a history of comorbid neurological conditions (eg, history of severe traumatic brain injury) that could potentially affect interpretation of neuroimaging findings were excluded.

Two independent control cohorts were used for comparative advanced imaging analytics. The first control cohort (control set 1) was designed to optimally match the high educational and professional status of the patients and consisted of demographically similar (in terms of age, ethnicity, and education) healthy adults, holding at least 1 college degree, and performing jobs that required dexterity and multitasking. To improve generalizability of the comparisons conducted, a second control cohort (control set 2) was assembled that consisted of healthy individuals with a broader spectrum of education and skills.

Neuroimaging Protocol

Neuroimaging for the patients was performed on a single Siemens 3T scanner (Magnetom Prismafit) and consisted of standard 3D FLAIR and T1- and T2-weighted series; a multiband, multishell dMRI; and an rs-fMRI, with a total acquisition time of less than 1 hour (see eAppendix 1 in the Supplement for details). Neuroimaging for control set 1 was acquired using the same protocol as that used for the patients. For control set 2, neuroimaging was originally acquired for another study on the same scanner but with a different imaging protocol. To determine that all control scans were from individuals without clinically significant underlying brain disorders, the scans were reviewed by a neuroradiologist; in the case of an abnormality, this assessment was reviewed with a neurologist to determine clinical relevance.

Key Points

Question Do advanced neuroimaging findings differ between US government personnel who experienced neurological signs and symptoms after potential exposure to directional phenomena in Havana, Cuba, and individuals not exposed to directional phenomena?

Findings In this study comparing 40 US government personnel with 48 healthy controls, advanced brain magnetic resonance imaging techniques revealed significant between-group differences in whole brain white matter volume, regional gray and white matter volume, cerebellar tissue microstructural integrity, and functional connectivity in the auditory and visuospatial subnetworks but not in the executive control subnetwork.

Meaning Neuroimaging findings differed between controls and US government personnel who experienced neurological signs and symptoms after potential directional phenomena exposure in Havana, Cuba, although the clinical relevance of these differences is uncertain and may require further study.

Each MRI scan individually underwent image preprocessing and stringent quality control (see eAppendix 2 in the Supplement for details of processing and quality control). Depending on the modality, different numbers of participants were excluded because their scans failed the stringent imaging quality control.

T1-weighted scans of both control cohorts were pooled (see eAppendixes 4, 5.4, and 5.7 in the Supplement for details). Diffusion MRI scans of both control cohorts were also combined using ComBat,[5] an imaging data harmonization strategy that eliminates the effect of different scanner parameters on the data while preserving biological effects (eAppendixes 4 and 7.5 in the Supplement). In rs-fMRI, only control set 1 was used, as no comparable data were available in control set 2.

Image Analytics Design and Outcome Measures

The main outcomes of interest were differences in (1) whole brain and regional brain tissue volume, (2) tissue microstructural integrity, and (3) functional connectivity of functional networks in patients compared with controls. The following measures were derived for analysis.

Brain Tissue Volume Maps

The T1-weighted images were used for volumetric analysis. Maps of white matter and gray matter tissue volumes were created relative to a reference template scan[6] using the T1-weighted scan. Multi-atlas segmentation was used to delineate gray matter, white matter, and cerebrospinal fluid, and deformable registration methods mapped the resultant regional tissue volumes to a standardized reference system for subsequent statistical analysis of volumetric patterns (see eAppendixes 2 and 3.1 in the Supplement for details). Mean regional volumes were computed for regions of the Neuromorphometrics atlas.[7]

Tissue Microstructural Integrity Maps

Diffusion tensor imaging[5,8] is a form of dMRI that uses multiple diffusion-weighted measurements along different gradient directions to characterize the differential diffusion of water molecules in the brain tissues. The water diffusion in each voxel in the brain is modeled by a rugby ball–shaped ellipsoid, called a tensor. The 3 axes of the ellipsoid provide the magnitude of water diffusivities along the directions of the axes. The shape of the ellipsoid is indicative of the extent of anisotropy (directionality) and ease of water diffusivity. The lengths of the axes can be combined to create different measures. The measure capturing diffusion along the long axis of fibers is called *axial diffusivity*, diffusion perpendicular to the long axis is termed *radial diffusivity*, and the average of all the axes is called *mean diffusivity*. A summary measure representative of the anisotropy or directionality of the tissue is *fractional anisotropy*. Additionally, a measure representative of the extracellular water in the brain, called *free water volume fraction*, can be derived using free water estimation.[9] Observed changes in these measures may result from changes in different factors like axonal packing density, axon caliber, axonal diameter, microglia, inflammation, and changes in extracellular and intracellular water and tissue architecture, making their bio-

logical interpretation challenging.[10,11] Because individual measures cannot independently and unambiguously identify the underlying cause, joint analysis is undertaken to indicate microstructural change. For this study, fractional anisotropy, mean diffusivity, radial diffusivity, axial diffusivity, and free water volume fraction were computed for all patients and controls for subsequent voxel-based and region-of-interest-based analysis. Mean microstructural measures were computed for regions defined in the JHU (Johns Hopkins University) atlas.[12] See eAppendixes 2 and 3.2 and eFigures 1 and 2 in the Supplement for details.

Functional Connectivity

The rs-fMRI data were used to create functional connectomes by computing the correlation coefficient of functional time series between pairs of regions. Subsequently, auditory, visuospatial, and executive control subnetworks pertaining to those functions were derived from the functional connectomes[13] (eAppendix 3.3 in the Supplement).

Additional Measures and Outcomes

Additional measures such as full brain structural connectivity from dMRI data and white matter hyperintensities from T2-weighted imaging data were assessed for differences between patients and controls.

Measures of Clinical Assessment Used for Correlation With Imaging

Only a subset of patients were referred to neuro-optometry, vestibular physical therapy, or both for further evaluation, based on clinical indications such as convergence insufficiency or abnormalities of static and dynamic balance on physical examination. This subgroup had quantitative clinical measures available for correlational analysis with imaging findings. Four scores that serve as measures of vestibular and oculomotor function and were obtained as part of the clinical evaluation were used to investigate potential correlation with imaging. Vestibular function was measured using the Sensory Organization Test[14] (range, 14-84; ≥70 indicates normal), which evaluates postural control and postural sway using computerized dynamic posturography. Assessment of oculomotor functions included 2 measures of vergence,[15,16] near point of convergence (range, 2.5-25 cm; ≤6 cm indicates normal) and positive fusional vergence (range, 6-40 prism diopters base-out; ≥20 prism diopters base-out indicates normal), as well as a measure of saccadic eye movement, the Developmental Eye Movement test[17] (range, 25-90 seconds; ≤30 seconds indicates normal).

Statistical Analysis

Hypotheses

Prespecified hypothesis-driven analyses were undertaken for brain tissue volume, tissue microstructural integrity, and functional connectivity.

- In brain volume analysis, the hypothesis was that there would be differences between patients and controls in overall white and gray matter volume, as well as regional differences in these measures.

- In the analysis of tissue microstructural integrity, due to clinical symptomatology suggesting cerebellar abnormalities, the primary hypothesis was that there would be differences in the cerebellum between patients and controls in mean diffusivity and fractional anisotropy, and the secondary hypothesis was that there would be differences in the cerebrum in mean diffusivity and in cerebral white matter in fractional anisotropy, axial diffusivity, radial diffusivity, and free water volume fraction. We chose to analyze the additional measures of axial diffusivity, radial diffusivity, and free water volume fraction in both the cerebellum and cerebrum only in the secondary hypothesis because of the small sample size.
- In functional connectivity analysis, based on the observed persistent neurological symptoms and signs, the primary hypothesis was that there would be a difference within the auditory, visuospatial, or executive control subnetworks of patients compared with controls, and the secondary hypothesis was that there would be differences within the visuospatial subnetwork, chosen because of clinical indication (balance and eye movement deficits).

In each of the 3 modalities, because a subset of patients had a remote history of concussion (prior brain injury), a secondary sensitivity analysis was performed excluding the prior brain injury group to avoid confounding due to the presence of any prior neurological insult. Another secondary sensitivity analysis was undertaken, when possible, to assess whether group differences found via the primary hypothesis were consistent when testing patients against each control group separately. Exploratory analyses were undertaken of whole-network structural connectivity, whole-network functional connectivity, and white matter hyperintensities to assess differences between patients and controls. Additional exploratory analyses were performed to investigate the correlation between clinical assessments of vestibular and oculomotor dysfunction and brain regions showing significant group differences in imaging.

Specifically, the analyses pertaining to the above hypotheses are as follows:

- The volumetric maps derived from T1-weighted images were interrogated for group differences at the voxel-wise level as well as the regional level.
- For tissue microstructural integrity, the primary hypothesis was interrogated voxel-wise and regionally. We divided the cerebellum into 12 gray matter and 2 white matter regions of interest based on the Yeo atlas.[18] The median value of the tissue integrity map was calculated for each region. The region-of-interest–based measurements of mean diffusivity for all 14 regions of interest were combined with the fractional anisotropy of the 2 white matter regions to interrogate the primary hypothesis with 16 region-of-interest–based statistical tests. The secondary hypothesis was interrogated at the voxel-wise level in the cerebrum (excluding cerebrospinal fluid voxels). The results of the voxel-wise analysis were assigned regional names by inspection by an expert who was blinded to group and confirmed by overlaying the JHU atlas.[12,19]
- The functional subnetwork data underwent statistical testing on the mean values for the auditory, executive control,

and visuospatial subnetworks to test the primary hypothesis. Secondary hypothesis tests were performed on every edge within the visuospatial subnetwork.

Statistical Modeling

Data underwent linear regression via ordinary least squares with terms for group, age, and sex (total brain volume was also included for analysis of volumetrics), and residuals were computed to produce demographically adjusted measurements. The normality of these residuals for each measure was tested using the Anderson-Darling test, and subsequent analysis was adjusted accordingly. Measures for which residual normality was supported were analyzed by linear regression. Group differences of voxel-wise tests were inspected as maps of *t* statistics and their associated *P* values. For region-of-interest tests, per-region estimates of group difference, 95% confidence intervals, and *P* values were calculated from the regression model. Statistical analysis of measures that showed departure from normality was performed using the Mann-Whitney *U* test on demographically adjusted residuals, and the rank-biserial correlation (a measure of effect size) was computed to show the magnitude of the association and the direction of the group difference. Effects of age and sex in these analyses were also assessed by inspection of the *t* statistics corresponding to the age and sex terms in the regression model. Multiple comparisons correction was undertaken by using the Benjamini-Hochberg procedure to control the false discovery rate. Only results of the primary hypotheses outlined above underwent correction for multiple comparisons using this procedure. For secondary hypotheses, sensitivity analyses, and exploratory analyses, statistical hypothesis tests were assessed at the uncorrected *P* < .05 level. Due to the potential for type I error, findings of these analyses should be interpreted as exploratory. Voxel-wise statistical tests were performed using AFNI (Analysis of Functional NeuroImages [National Institutes of Health/Medical College of Wisconsin]) 3dRegAna version 17.2.10.[20] Region-of-interest–based regression analysis, Anderson-Darling and Mann-Whitney *U* tests, multiple comparisons correction, and calculation of effect sizes were performed using in-house scripts in Python version 2.7 using SciPy version 1.0.0 and Statsmodels version 0.8.0.

Correlation of Imaging With Clinical Scores

Exploratory analysis was undertaken to investigate the correlation between the imaging measures defined above and the quantitative clinical scores (ie, Sensory Organization Test, near point of convergence, positive fusional vergence, and Developmental Eye Movement test) in the subgroup of patients with available clinical measures of vestibular and oculomotor function (data from controls were not included in the correlational analysis). As vestibular and oculomotor function require multisensory integration comprising the auditory and visual systems[21] and the cerebellum, the scores for their assessment can be affected by deficits in various brain networks, making it challenging to identify specific brain regions for correlation with imaging. Therefore, correlations with all brain regions were evaluated at the expense of

Table. Ages of Patient and Control Cohorts

	Age, Mean (SD)		
	Patients	Control Set 1	Control Set 2
All participants			
Male	37.7 (8.6) (n=23)	39.2 (9.3) (n=13)	37.5 (9.3) (n=22)
Female	44.1 (10.0) (n=17)	40.5 (4.2) (n=8)	30.9 (12.2) (n=9)
Patients with prior brain injury			
Male	47.0 (9.0) (n=9)	NA	NA
Female	39.0 (8.8) (n=3)	NA	NA
Patients with clinical scores			
Male	38.8 (7.0) (n=17)	NA	NA
Female	43.5 (9.6) (n=11)	NA	NA
Data sets passing volumetric quality control			
Male	37.7 (8.6) (n=23)	39.2 (9.3) (n=13)	38.0 (9.2) (n=20)
Female	44.1 (10.0) (n=17)	40.5 (4.2) (n=8)	30.4 (12.6) (n=7)
Data sets passing diffusion tensor imaging quality control			
Male	37.8 (7.9) (n=20)	39.2 (9.3) (n=13)	36.4 (9.6) (n=12)
Female	44.1 (10.0) (n=17)	40.5 (4.2) (n=8)	29.4 (12.1) (n=8)
Data sets passing rs-fMRI quality control			
Male	37.7 (8.6) (n=18)	39.0 (9.7) (n=12)	NA
Female	45.0 (10.3) (n=15)	40.5 (4.2) (n=8)	NA

Abbreviations: NA, not applicable; rs-fMRI, resting-state functional magnetic resonance imaging.

losing statistical significance due to increased comparisons. The correlation was modeled as a regression with age, sex, and clinical score in the model. For volume, intracranial volume was used as an additional regressor. The association of the clinical score was reported as the β coefficient of this model, interpreted as the units of change in an imaging measure per unit increase in clinical score. To understand the relevance of the correlations, imaging metrics in regions that showed correlations with clinical measures were then considered in light of whether there were between-group differences among patients and controls in terms of the imaging metric in that specific region. For rs-fMRI, the total connectivity of visuospatial, auditory, and executive control networks was correlated with the clinical measures with the same model. Correlation analyses were performed using scripts written in Python 2.7 using Statsmodels version 0.8.0. In total, 564 correlation analyses of volume (141 regions and 4 clinical measures), 2816 correlation analyses of microstructural indices (176 regions, 4 indexes, and 4 clinical measures), and 12 correlation analyses of functional connectivity (3 subnetworks and 4 clinical measures) were performed.

brain injury with a left temporal lobe contusion, congenital neurological insult, and pseudotumor cerebri, respectively) and 1 individual who did not consent to this neuroimaging study were excluded.

Among the 40 patients included, 12 had a remote history of concussion, all with resolution of symptoms prior to directional phenomena exposure, and all 12 were included. The mean age of patients was 40.4 years, there were 23 men and 17 women, and advanced neuroimaging was performed a median of 188 days (range, 4-403 days) after initial suspected exposure. Among the 40 patients included, 28 were referred for further vestibular and/or oculomotor evaluations as part of clinical care and had clinical data available for correlations with neuroimaging findings.

The 2 control groups originally included 52 participants, but only 48 had neuroimaging data that were of sufficient quality to be included. Among the 48 controls (mean age, 37.6 years; 33 men and 15 women), there were 21 individuals in control set 1 (mean age, 39.7 years; 13 men and 8 women) and 27 individuals in control set 2 (mean age, 36.0 years; 20 men and 7 women). The **Table** contains additional detail regarding participant demographic information and imaging quality control.

Results

A total of 44 patients were referred for clinical evaluation and treatment following potential exposure to directional phenomena while serving in Havana, Cuba, between late 2016 and May 2018. Advanced neuroimaging was performed for 40 of the 44 patients (including 20 of the 21 individuals described in the previous report[2]). Three individuals with comorbid neurological conditions (history of moderate to severe traumatic

Volumetric Analysis

Whole brain white matter volume of patients was significantly smaller than that of controls (patients: 542.22 cm^3; controls: 569.61 cm^3; difference, −27.39 [95% CI, −37.93 to −16.84] cm^3; $P < .001$). There was no significant difference in whole brain gray matter volume (patients: 698.55 cm^3; controls: 691.83 cm^3; difference, 6.72 [95% CI, −4.83 to 18.27] cm^3; $P = .25$). There were widespread voxel-wise

**Figure 1. Volumetric Differences Between Patients and Controls**
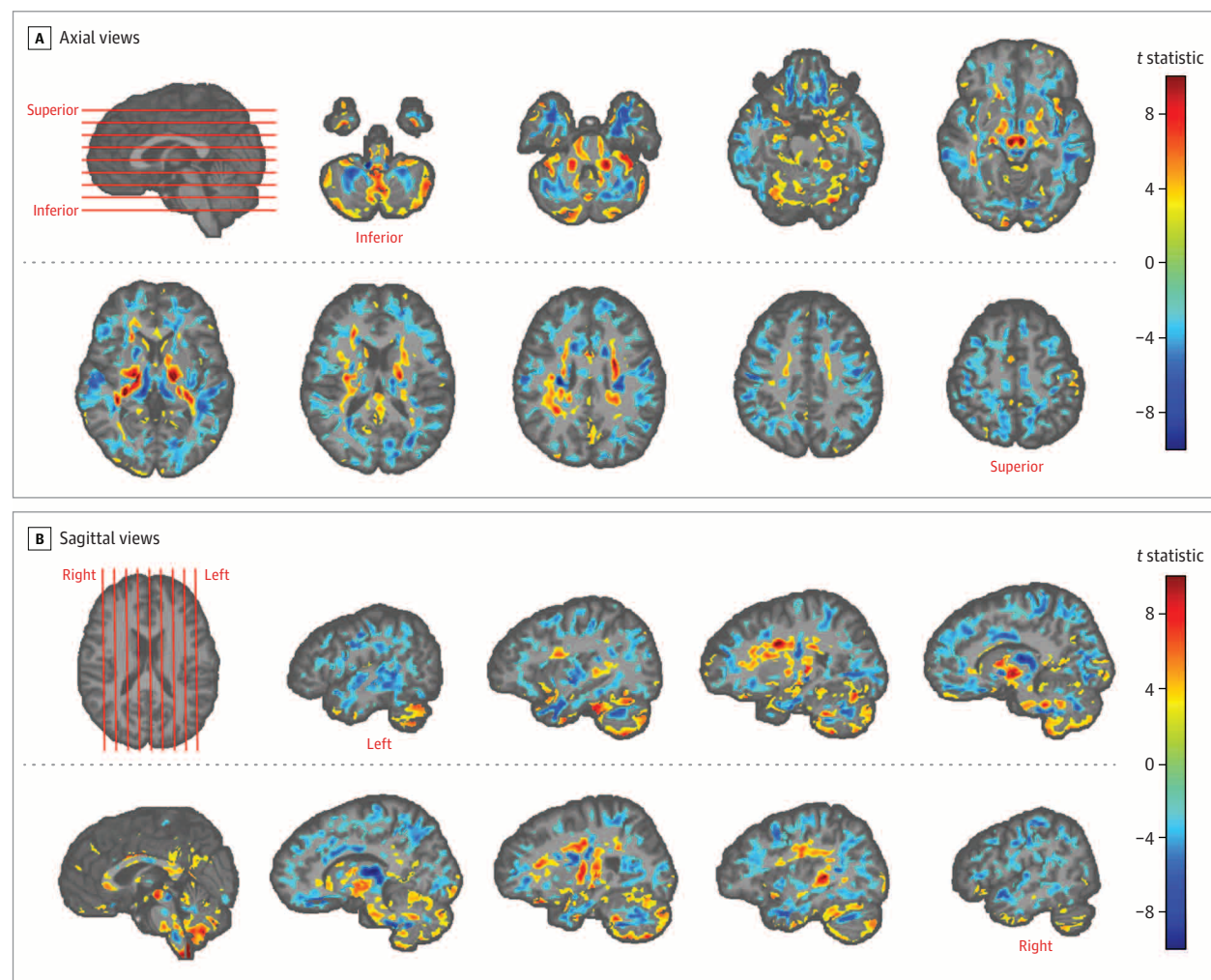
Maps of white matter and gray matter tissue volume were created for each participant using T1-weighted images and registering them to a template. The act of registering to a common space results in a relative measure of local volume at each location in the brain, called a volumetric map. Volumetric maps of participants were compared using an ordinary least squares regression model with terms for group, age, sex, and intracranial volume, implemented in AFNI (Analysis of Functional NeuroImages) 3dRegAna version 17.2.10. Results of the statistical analysis of the volumetric difference between patients and controls are shown by overlaying the *t*-statistic maps of group difference on a template brain in various views. For panel A, axial views of the brain, and panel B, sagittal views of the cerebellum and cerebrum, locations of chosen slices are shown by red lines on the template brain (first image in each panel). Only voxels that were significantly different in volume between patients and controls after false discovery rate correction are shown, with the color bars on the right encoding the *t* statistic, ranging from −10 to 10. Yellow to red voxels in the slices are representative of significantly higher volume in patients vs controls; cyan to blue voxels are representative of significantly lower volume in patients vs controls. Gray matter volume differences were most prominent in the cerebellum. In the cerebrum, there was higher white matter volume in the projection fibers and lower white matter volume in the association or U fibers. Voxels with no significant difference have no value in the statistical comparison map and were left blank.

differences in the brains of patients compared with controls in the voxel-wise analysis, both in white matter and gray matter (**Figure 1**). These differences resulted in a pattern of greater white matter volume in the projection fibers (especially corona radiata and the internal capsule) and less white matter volume in the association fibers (also called U fibers). Compared with controls, patients had greater volume in the ventral diencephalon (patients: 4.90×10^3 mm^3; controls: 4.70×10^3 mm^3; difference, 201.64 [95% CI, 80.59-322.69] mm^3; $P = .01$). Patients had smaller volume in the frontal lobe white matter (patients: 9.76×10^4 mm^3; controls: 1.03×10^5 mm^3; difference, -5.57×10^3 [95% CI,

-8.21×10^3 to -3.13×10^3] mm^3; $P < .001$), occipital lobe white matter (patients: 2.41×10^4 mm^3; controls: 2.60×10^4 mm^3; difference, -1.88×10^3 [95% CI, -2.82×10^3 to -9.46×10^2] mm^3; $P < .001$), and parietal lobe white matter (patients: 5.11×10^4 mm^3; controls: 5.45×10^4 mm^3; difference, -3.41×10^3 [95% CI, -4.70×10^3 to -2.12×10^3] mm^3; $P < .001$). In the cerebellums of patients, gray matter showed greater volume (patients: 5.47×10^4 mm^3; controls: 5.01×10^4 mm^3; difference, 4.54×10^3 [95% CI, 2.59×10^3 to 6.49×10^3] mm^3; $P < .001$), with neighboring white matter showing smaller volumes (patients: 1.46×10^4 mm^3; controls: 1.57×10^4 mm^3; difference, -1.04×10^3 [95% CI,

Figure 2. Differences in Tissue Microstructural Integrity in the Cerebellum
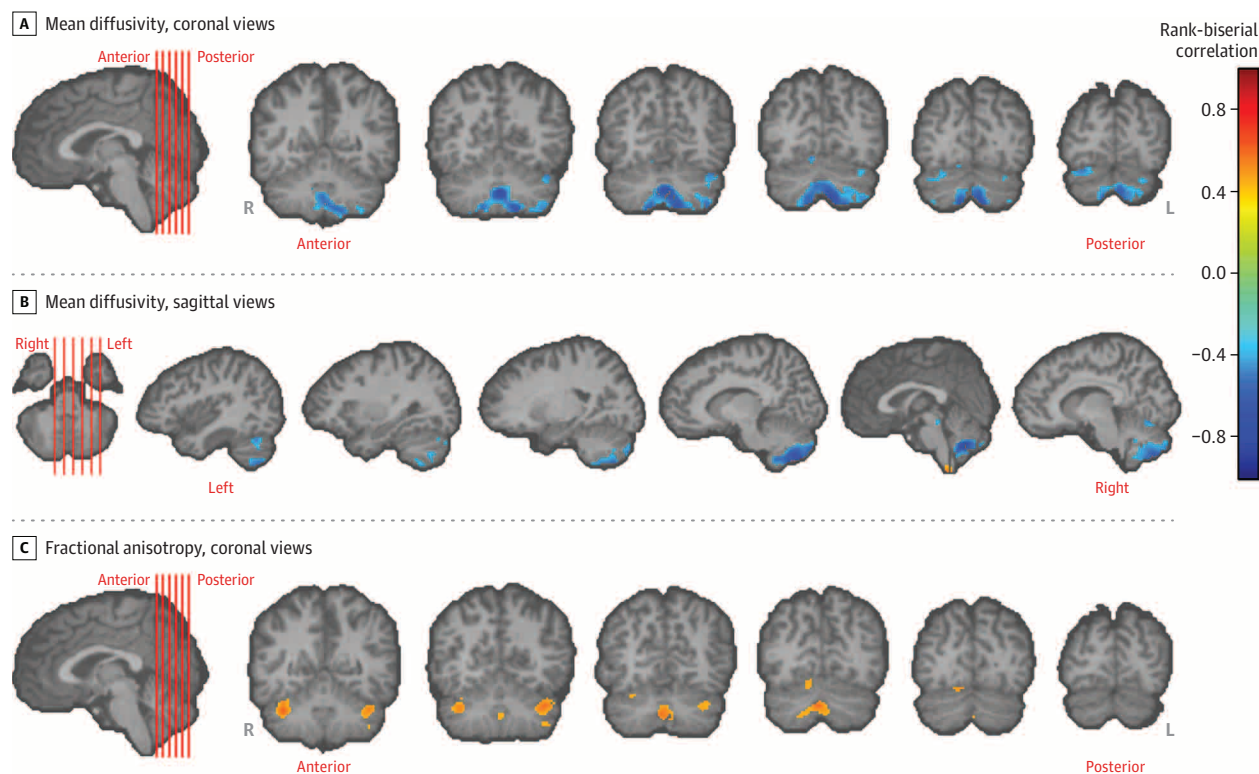
Tissue microstructural integrity is represented by various diffusion tensor indexes, such as mean diffusivity and fractional anisotropy. Results of voxel-based statistical analysis of the diffusion tensor indexes are shown, testing the primary hypothesis with a Mann-Whitney U test. The primary hypothesis was that there were differences in tissue integrity in the cerebellums of patients vs controls. Statistical maps of difference in terms of rank-biserial correlation (a measure of effect size; range, −1 to 1) are overlaid on the cerebellum and brainstem of a template brain to which all participants have been registered. Only voxels with significant difference (false discovery rate–corrected $P < .05$) in the cerebellum and brainstem are shown. Locations of chosen slices are shown by red lines on the template brain (first image in each panel). The cerebrum is shown in template brains for completion, but those locations were not tested according to the primary hypothesis of this study. The color bar encoding rank-biserial correlation applies to all panels. In panel A (coronal views) and panel B (sagittal views), regions of significantly lower mean diffusivity in the cerebellum in patients vs controls are shown in blue. In panel C (coronal views), regions in the cerebellum with significantly higher fractional anisotropy in patients are shown in orange.

$−1.59 × 10^3$ to $−4.99 × 10^2$] mm³; $P < .001$) compared with controls. All results were false discovery rate corrected.

Results showing percentage difference in volume are shown in eAppendix 5.5 and eFigure 6 in the Supplement. Region-wise results are shown in eAppendix 5.2 and eFigure 3 in the Supplement. Excluding the prior brain injury group did not alter the pattern of the findings (eAppendix 5.3 and eFigure 4 in the Supplement). In comparisons of patients with each control group separately, differences were maintained in the same regions and direction, and there were no significant differences between the 2 control groups affecting the results (eAppendix 5.4 and eFigure 5 in the Supplement).

Analysis of Microstructural Tissue Metrics

Microstructural tissue metrics of the gray matter exhibited nonnormal residuals, and differences between patients and controls were assessed with the Mann-Whitney U test. Results of testing the primary hypothesis in the cerebellum are presented in **Figure 2** and results of testing the secondary hypothesis in the cerebrum in **Figure 3**. As shown in

Figure 2, A and B, the inferior vermis of the cerebellum had significantly lower mean diffusivity in patients compared with controls (patients: $7.71 × 10^{-4}$ mm²/s; controls: $8.98 × 10^{-4}$ mm²/s; difference, $−1.27 × 10^{-4}$ [95% CI, $−1.93 × 10^{-4}$ to $−6.17 × 10^{-5}$] mm²/s; $P < .001$), with a higher fractional anisotropy ratio in the vermis (patients: 0.21; controls: 0.19; difference, 0.022 [95% CI, 0.014-0.029]; $P < .001$) and in other regions (Figure 2C). These results were false discovery rate corrected. Region-of-interest–based secondary analysis of the primary hypothesis in the cerebellum showed lower mean diffusivity in the regions pertaining to limbic, dorsal attention, somatomotor, default, and frontoparietal functions, with the entire vermis being implicated (eAppendix 7.2, eFigure 13, and eTable 5 in the Supplement). Analyses of the cerebrum according to the secondary hypothesis of microstructural indexes indicated lower mean diffusivity and axial diffusivity in the anterior limb of the internal capsule, inferior colliculi, superior cerebral peduncle, and occipital white matter (not false discovery rate corrected) (Figure 3; eFigure 21 in the Supplement).

Figure 3. Differences in Tissue Microstructural Integrity in the Cerebrum

A   Mean diffusivity, sagittal views

B   Fractional anisotropy, sagittal views

Rank-biserial correlation

0.8

0.4

0.0

−0.4

−0.8
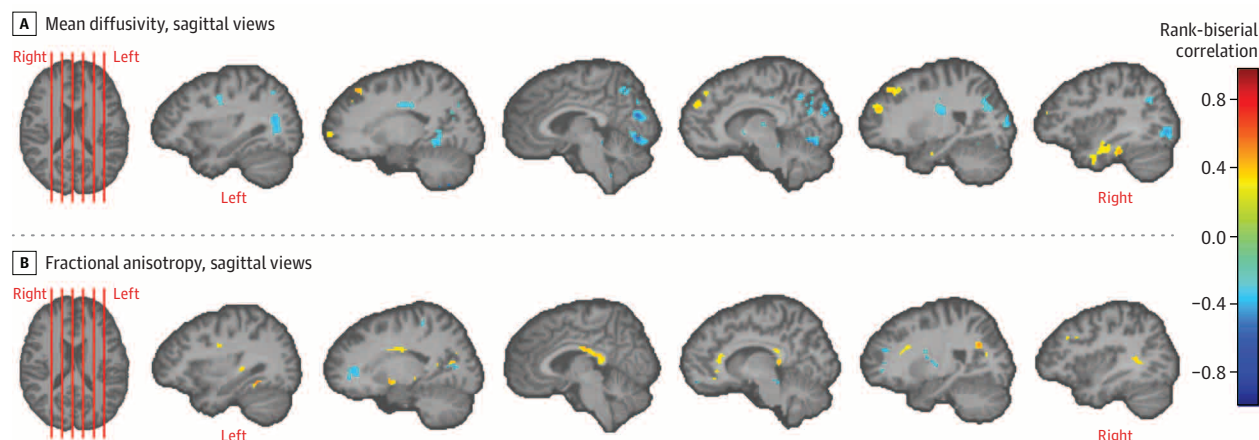
Results of a voxel-based analysis of tissue microstructural integrity measures of fractional anisotropy and mean diffusivity in the cerebrum using Mann-Whitney *U* test are shown. This pertains to the testing of the secondary hypothesis that there were differences in tissue integrity in the cerebrums of patients as compared to controls. The statistical maps are color coded using rank-biserial correlation (a measure of effect size; range, −1 to 1) as shown in the color bar, which applies to both panels. These maps are overlaid on a template brain, with only the voxels showing differences (uncorrected *P* < .05) color coded. Results in the cerebellum are shown in Figure 2. Representative slices are shown in panel A for lower mean diffusivity in patients vs controls in 6 sagittal views of the brain (regions include anterior limb of the internal capsule and occipital white matter) and panel B for higher fractional anisotropy in patients vs controls in 6 sagittal views of the brain (regions include splenium of the corpus callosum). Locations of these chosen slices are shown by red lines on the template brain (first image in each panel).

There was higher fractional anisotropy in the colliculi and the splenium of patients vs controls.

In analyses pertaining to secondary hypotheses, lower axial diffusivity, radial diffusivity, and free water volume fraction in the cerebellum was found in patients vs controls, especially in the inferior vermis (eAppendix 7.1 and eFigures 10, 11, 12, and 21 in the Supplement).

In sensitivity analyses, the direction of the group differences remained consistent when individuals with prior brain injury were excluded from the statistical analysis (eAppendix 7.3 and eFigure 14 in the Supplement). These analyses combined both control groups after harmonization (eAppendix 7.5 and eFigure 16 in the Supplement).[5] There were no significant differences between the 2 control groups. Additionally, results were consistent when the 2 control groups were treated separately (eAppendix 7.4 and eFigure 15 in the Supplement).

Functional Connectivity Changes

Functional connectivity measures met the criterion for normality. As shown in **Figure 4**, the auditory subnetwork (patients: 0.45; controls: 0.61; difference, −0.16 [95% CI, −0.26 to −0.05]; *P* = .003) and the visuospatial subnetwork (patients: 0.30; controls: 0.40; difference, −0.10 [95% CI, −0.16 to −0.04]; *P* = .002) showed significantly lower connectivity in patients (false discovery rate corrected). There was no significant difference in the executive control subnetwork (patients: 0.24; controls: 0.25; difference, −0.016 [95% CI, −0.04 to 0.01]; *P* = .23). Analysis of the secondary hypothesis revealed lowered interregional functional connectivity within the visuospatial subnetworks of patients vs controls (non–false discovery rate-corrected *P* < .05), as
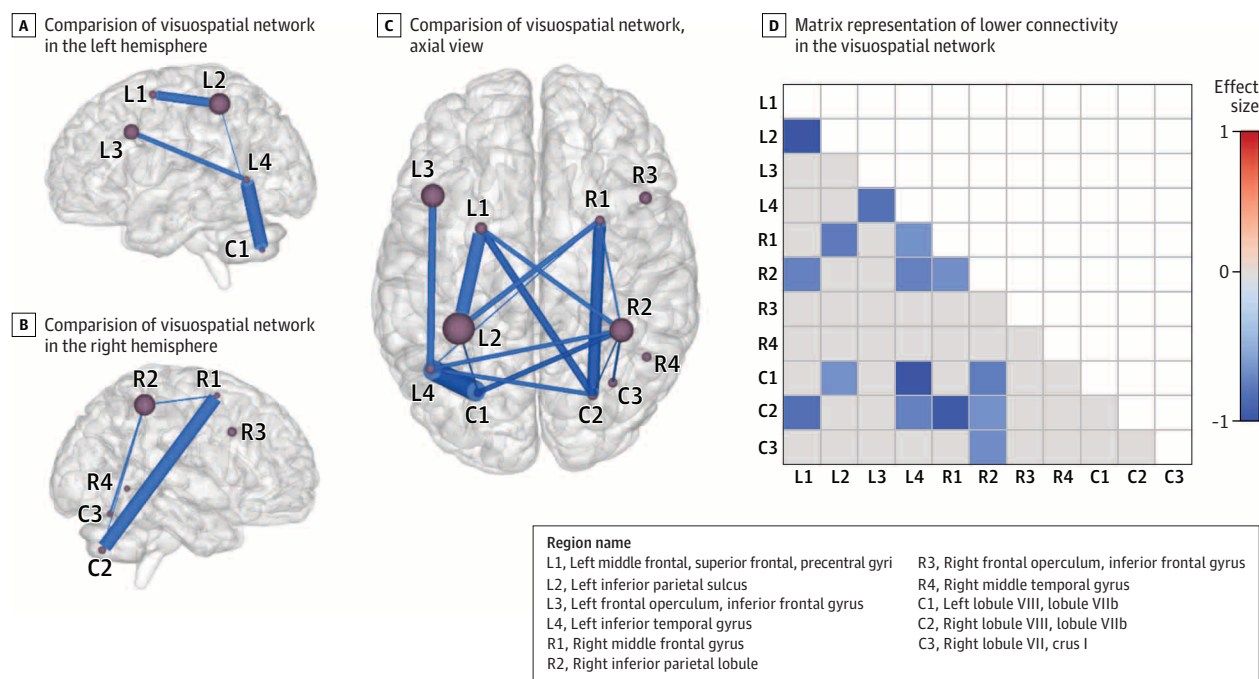
Figure 4. Comparisons of Functional Networks Between Patients and Controls
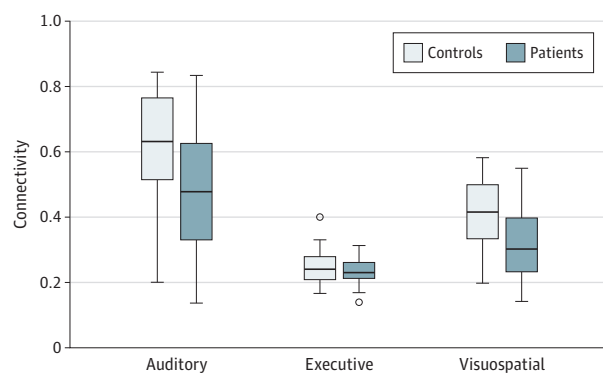
Results of testing the primary hypothesis that there were differences between patients and controls in auditory, executive control, and visuospatial subnetworks of the functional connectome. Linear regression was used with age and sex as covariates. The box tops and bottoms indicate interquartile ranges; whiskers extend to the furthest data points that lie within 1.5 interquartile ranges below the 25th and above the 75th percentiles; circles indicate outliers; and horizontal lines inside the boxes indicate medians. Patients had significantly lower connectivity in auditory and visuospatial subnetworks vs controls (false discovery rate–corrected *P* < .05). There was no significant difference in the executive control subnetwork.

shown in **Figure 5**. For results of exploratory analysis of whole-network functional connectivity, see eAppendix 9.1 and eFigure 18 in the Supplement. Sensitivity analysis of the auditory and visuospatial networks also showed lower connectivity in patients when the analysis was repeated by

Figure 5. Comparisons of Visuospatial Subnetwork Functional Connectivity Between Patients and Controls

Region name
L1, Left middle frontal, superior frontal, precentral gyri
L2, Left inferior parietal sulcus
L3, Left frontal operculum, inferior frontal gyrus
L4, Left inferior temporal gyrus
R1, Right middle frontal gyrus
R2, Right inferior parietal lobule
R3, Right frontal operculum, inferior frontal gyrus
R4, Right middle temporal gyrus
C1, Left lobule VIII, lobule VIIb
C2, Right lobule VIII, lobule VIIb
C3, Right lobule VII, crus I

Results of testing the secondary hypothesis that there were functional connectivity differences between patients and controls within the connections of the visuospatial subnetwork. Panels A, B, and C show the results of comparing the visuospatial network of patients and controls. Nodes (spheres) represent the regions in the visuospatial network and are sized in proportion to the volume of the region in the Greicius atlas (a standardized brain atlas); thickness of blue lines connecting these nodes represents magnitude of mean difference in functional connectivity between regions. Lower connectivity in the visuospatial network in patients is shown in the left (panel A) and right (panel B) hemispheres; only intrahemispheric connections are shown for clarity. An axial view from the top (panel C) shows lower connectivity (uncorrected $P < .05$) including intrahemispheric and interhemispheric connections. Panel D shows the matrix representation of lower connectivity (uncorrected $P < .05$) in the visuospatial network, color coded with the effect sizes (Cohen d) of the mean difference in connection strength between patients and controls. Cells shown in gray were not significantly different between patients and controls. Cells shown in white were not reported because the matrix is symmetric about its diagonal.

excluding individuals with prior brain injury (eAppendix 9.2 and eFigure 19 in the Supplement).

Clinical Correlations

Correlations of neuroimaging findings with clinical signs were assessed among the 28 patients with vestibular and/or oculomotor data available. eTable 3 in the Supplement provides a distribution of the clinical scores of patients.

In the right and left ventral diencephalon, where there was a significant group difference in volume, a worse score on near point of convergence correlated with greater volume (right ventral diencephalon: adjusted $R^2 = 0.72$; β = 34.48 [95% CI, 0.24-68.72]; $P = .05$; left ventral diencephalon: adjusted $R^2 = 0.72$; β = 37.40 [95% CI, 2.07-72.72]; $P = .04$). Other brain regions that showed differences in volume between groups did not have any significant correlation with clinical scores. Several regions with non-statistically significant group differences in volume also showed correlations, but these correlations did not survive multiple comparisons correction. The complete list of regions and their correlations can be found in eAppendix 11 and eTable 6 in the Supplement.

For the microstructural MRI measures, in the cerebellum, which was a region of significant group difference and was

the focus of the primary hypothesis of the tissue microstructure analysis, a higher mean fractional anisotropy of right hemisphere cerebellar gray matter correlated with a decrease in positive fusional vergence (adjusted $R^2 = 0.18$; β = -6.5×10^{-40} [95% CI, -1.22×10^{-3} to -8.31×10^{-5}]; $P = .03$) and a lower mean diffusivity with a decrease in Sensory Organization Test score (adjusted $R^2 = 0.17$; β = 4.94×10^{-6} [95% CI, 3.65×10^{-7} to 9.51×10^{-6}]; $P = .04$). Several regions with nonstatistically significant differences in microstructure also showed correlation. Details are shown in eAppendix 11 and eTable 7 in the Supplement.

For functional connectivity, there were no significant correlations between prespecified subnetworks and clinical scores.

Additional Analyses

There were no significant differences in whole-network structural connectivity (eAppendix 8 in the Supplement), or functional connectivity (eAppendix 9.1 in the Supplement) between patients and controls. There was no significant difference in white matter hyperintensity ratings (eAppendix 10 in the Supplement). Correlations were not undertaken with structural connectivity measures, full-network functional connectivity measures, or white matter hyperintensity counts, as no significant differences in these measures were found.

Discussion

Advanced brain neuroimaging of a group of US government personnel potentially exposed to directional phenomena while working in Havana, Cuba, showed significant differences in whole brain white matter volume, regional gray and white matter volume, cerebellar tissue microstructural integrity, and functional connectivity in the auditory and visuospatial subnetworks compared with controls. These findings suggest that there may be differences in brain structure involving several different brain regions as well as in some functional brain networks.

The finding of significantly less white matter volume in patients compared with controls was also reflected in some regional differences. Voxel-wise white matter volumetric differences also differed between projection and association fibers. This may indicate that there were differences in axonal volume, myelin-to-axon ratio, or free water volume fraction. These patterns of volumetric differences do not conform readily to any established mechanisms of pathogenesis, nor do they form an anatomical basis for a specific behavioral dysfunction observed in other brain disorders.

In the microstructural measures derived from DTI, patients demonstrated differences compared with controls in both cerebellar and cerebral regions, with lower mean diffusivity, radial diffusivity, and axial diffusivity and higher fractional anisotropy in patients. This is in contrast to the increased mean diffusivity and decreased fractional anisotropy observed in other brain disorders, such as traumatic brain injury.[22,23] There was also lower free water volume fraction and lower mean diffusivity, contrary to what is observed due to axonal swelling in acquired brain injuries such as traumatic brain injury and stroke.[23] Lower axial diffusivity could be the result of postinjury gliosis that causes a hindrance to water movement or traumatically induced formation of undulations along axons.[24,25] In conjunction with this, a higher fractional anisotropy could be due to a loss of intracellular water, compaction of axons, or both. Notably, the latter has been observed in experimental models of traumatic brain injury due to ultrastructural changes.[25]

The presence of cerebellar differences in terms of tissue volume and microstructure in the patients may have important clinical implications because involvement of this region is associated with vestibular and oculomotor dysfunction, which was observed in a subset of the patients. The prominently different cerebellar areas included the vermis, which receives visual and auditory inputs, and the vestibulocerebellum, which receives vestibular inputs. These differences may be associated with the differences observed in volumetric changes between association and projection fibers, due to the preferential involvement of deep white matter projection fibers in the vestibular system and association fibers in integrating oculomotor function. In the analysis of tissue microstructure of the cerebellum, the significant differences in mean diffusivity and free water volume fraction point to lower water content in patients compared with controls. Although little is known about how changes in cellular water

are reflected in volume, the pattern of higher superficial gray matter volume, lower deep gray matter volume, and lower white matter volume could be explained by differential changes in water content in the molecular, Purkinje, and granular layers of the cerebellum. In addition to the anatomical view of the cerebellum, analysis of an imaging-based functional parcellation of the cerebellum revealed significantly lower mean diffusivity in regions linked to motor, frontoparietal, and default mode network functionality.

Significantly lower functional connectivity was observed in the auditory and visuospatial networks in patients compared with controls. These functional imaging differences were supported by the lower tissue integrity measures of mean diffusivity, radial diffusivity, axial diffusivity, and free water volume fraction in the inferior colliculi, which are linked to auditory and vestibular function. Although some patients demonstrated clinical deficits in executive functioning, no significant difference was found in the executive control subnetwork. A focused investigation of the visuospatial network showed involvement of the frontal supplemental and parietal eye fields and the dorsolateral prefrontal cortex, which are implicated in vergence and vestibular and saccade functioning.

In exploratory analyses, some correlations were observed between neuroimaging metrics and quantitative measures of vestibular and oculomotor dysfunction that were obtained clinically for a subset of 28 patients with neurological signs and symptoms that required subspecialty evaluation. In the right and left ventral diencephalon, where there was a significant group difference in volume, worse scores on near point of convergence correlated with greater volume in patients compared with controls. In the Neuromorphometrics atlas,[7] the ventral diencephalon is the anatomical name given to a group of structures that are difficult to distinguish from each other in standard MRI images, including the hypothalamus, mammillary body, subthalamic nuclei, substantia nigra, red nucleus, lateral geniculate nucleus, and medial geniculate nucleus. White matter areas such as the zona incerta, cerebral peduncle (crus cerebri), lenticular fasciculus, and medial lemniscus are also included in this area. The optic tract is also included in this area in the most anterior extent. In the cerebellum, lower mean diffusivity in patients compared with controls correlated with a worse score on the Sensory Organization Test, and higher fractional anisotropy in patients correlated with a worse positive fusional vergence score. The strength of correlation (R^2) of these diffusion-based tissue integrity measures with clinical scores was relatively weak. These correlations suggest a potential neuroanatomical basis of the observed neurological manifestations in these patients. However, this analysis must be interpreted in light of the limitation that numerous clinical and imaging correlations were evaluated, including clinical findings that showed no correlation with the imaging metrics or that showed correlation with imaging metrics that were not significantly different between groups. Thus, given issues related to multiple comparisons in the absence of predefined hypotheses, the relatively weak correlations observed for some metrics, and the absence of correlation with functional connectivity metrics

entirely, the clinical implications of the neuroimaging differences remain uncertain.

Imaging-based correlative studies need specifically hypothesized regions for clinical correlation and are rendered challenging by the complex nature of networks that could also be involved in the observed neurological dysfunction, as is the case for vestibular and oculomotor dysfunction. The diffuse nature of imaging differences, compounded by the heterogeneity of the clinical scores and their nonspecificity, may be confounding factors in any such correlation. This is especially challenging in a clinical sample in which patients did not receive clinical testing uniformly.

This was further complicated by the small number of patients and large degree of heterogeneity arising from multiple sources, including (1) difficulty in determining the presence or absence of an "exposure" beyond clinical history; (2) not knowing the character or relative "dose" of the potential exposure; (3) a highly varying time interval between the reported exposure and the clinical and MRI evaluations; (4) the existence of premorbid conditions and routine health problems; and (5) varying degrees of clinical symptom severity at the time of clinical evaluation, leading to different clinical treatment and intervention paradigms.

Limitations

This study has several limitations. First, the effort was not designed as a research study but was undertaken retrospectively, using clinically acquired data and measures of deficit assessment. Second, the ideal control cohort, composed of unaffected personnel who were identical to those deployed in Cuba, was not feasible to obtain. Although the controls recruited for the study were matched on age and sex, and generally matched on race/ethnicity, education, and multifunctional lifestyle of the patients, factors like blood pressure, bilingualism, and life experiences could not be matched. Race/ethnicity was not used as a covariate in the statistical analysis due to the small sample size. The race/ethnicity characteristics of the patient cohort cannot be revealed because of privacy and anonymity. A second independent control cohort was used to further ensure reproducibility of the results and mitigate any sampling bias that may have affected control set 1. Third, the analysis involved a small sample with high heterogeneity, compounded by clinical (as opposed to research) neuroimaging acquisition. In the absence of a common clinical severity score due to varied symptomatology, the cohort cannot be subdivided. Therefore, the findings represent group-level statistical differences

as opposed to individual changes that may be highly variable. Additionally, it cannot be determined whether the differences among the patients are due to individual differences between patients or differences in level and degree of exposure to an uncharacterized directional phenomenon. Fourth, because the patients have undergone neurological rehabilitation, the imaging findings may be representative of brain changes associated with the rehabilitation or compensatory changes in a recovering brain. Although this hampers future replication studies, complementary findings across various MRI measures, as undertaken in this study, are in themselves a form of replication in such a unique and small sample. Fifth, the tissue integrity measures of fractional anisotropy, mean diffusivity, radial diffusivity, and axial diffusivity are gross representations of tissue microstructure, to the extent that microstructural tissue properties can be captured by in vivo MRI protocols. However, these measures have been used for investigating various pathologies, as described above. Investigation of other microstructure measures, like axon diameter, requires advanced dMRI acquisition commonly acquired in dedicated research MRI acquisitions, and is therefore beyond the scope of the current clinical acquisition. In DTI, the macroresolution of acquisition means that the indexes are only a representation of the underlying microstructural changes and tissue integrity. The underlying mechanisms of axonal injury, myelin changes, or free water changes are challenging to disentangle in group-based statistical results. Sixth, image analysis methods have limitations. Segmentation methods quantify the volume of "gray-appearing" and "white-appearing" tissue. Although the former is known to correlate strongly with neuronal cell bodies and the latter to reflect axonal and myelin volumes, various pathological processes like axonal death, demyelination, and dehydration, among other processes, affect them.

Conclusions

Among US government personnel in Havana, Cuba, with potential directional phenomena exposure, compared with healthy controls, advanced brain MRI techniques revealed significant neuroimaging differences in whole brain white matter volume, regional gray and white matter volume, cerebellar tissue microstructural integrity, and functional connectivity in the auditory and visuospatial subnetworks but not in the executive control subnetwork. The clinical importance of these differences is uncertain and may require further study.

REFERENCES

1. US Senate Committee on Foreign Relations. Subcommittee hearing: attacks on US diplomats in Cuba. January 9, 2018. https://www.foreign.senate.gov/hearings/attacks-on-us-diplomats-in-cuba-response-and-oversight-010918. Accessed January 10, 2018.

2. Swanson RL II, Hampton S, Green-McKenzie J, et al. Neurological manifestations among US government personnel reporting directional audible and sensory phenomena in Havana, Cuba. JAMA. 2018;319(11):1125-1133. doi:10.1001/jama.2018.1742

3. Basser PJ, Mattiello J, LeBihan D. Estimation of the effective self-diffusion tensor from the NMR spin echo. J Magn Reson B. 1994;103(3):247-254. doi:10.1006/jmrb.1994.1037

4. Tuch DS. Diffusion MRI of Complex Tissue Structure [thesis]. Cambridge, MA: Harvard University and Massachusetts Institute of Technology; 2002.

5. Fortin JP, Parker D, Tunç B, et al. Harmonization of multi-site diffusion tensor imaging data. Neuroimage. 2017;161:149-170. doi:10.1016/j.neuroimage.2017.08.047

6. Davatzikos C, Genc A, Xu D, Resnick SM. Voxel-based morphometry using the RAVENS maps: methods and validation using simulated longitudinal atrophy. Neuroimage. 2001;14(6):1361-1369. doi:10.1006/nimg.2001.0937

7. Neuromorphometrics Inc. Multi subject atlas using brain color labeling protocol. https://scalablebrainatlas.incf.org/human/NMM1103. Accessed March 7, 2019.

8. Basser PJ, Mattiello J, LeBihan D. MR diffusion tensor spectroscopy and imaging. Biophys J. 1994;66(1):259-267. doi:10.1016/S0006-3495(94)80775-1

9. Ould Ismail AA, Parker D, Hernandez-Fernandez M, et al. Characterizing peritumoral tissue using free water elimination in clinical DTI. In: Brainlesion: Glioma, Multiple Sclerosis, Stroke and Traumatic Brain Injuries. Cham, Switzerland: Springer; 2019:123-131. BrainLes 2018: Lecture Notes in Computer Science volume 11383.

10. Armstrong RC, Mierzwa AJ, Marion CM, Sullivan GM. White matter involvement after TBI: clues to axon and myelin repair capacity. Exp Neurol. 2016;275(pt 3):328-333. doi:10.1016/j.expneurol.2015.02.011

11. Aung WY, Mar S, Benzinger TL. Diffusion tensor MRI as a biomarker in axonal and myelin damage. Imaging Med. 2013;5(5):427-440. doi:10.2217/iim.13.49

12. Oishi K, Faria A, Jiang H, et al. Atlas-based whole brain white matter analysis using large deformation diffeomorphic metric mapping: application to normal elderly and Alzheimer's disease participants. Neuroimage. 2009;46(2):486-499. doi:10.1016/j.neuroimage.2009.01.002

13. Shirer WR, Ryali S, Rykhlevskaia E, Menon V, Greicius MD. Decoding subject-driven cognitive states with whole-brain connectivity patterns. Cereb Cortex. 2012;22(1):158-165. doi:10.1093/cercor/bhr099

14. Alahmari KA, Marchetti GF, Sparto PJ, Furman JM, Whitney SL. Estimating postural control with the balance rehabilitation unit: measurement consistency, accuracy, validity, and comparison with dynamic posturography. Arch Phys Med Rehabil. 2014;95(1):65-73. doi:10.1016/j.apmr.2013.09.011

15. Gallaway M, Scheiman M, Mitchell GL. Vision therapy for post-concussion vision disorders. Optom Vis Sci. 2017;94(1):68-73. doi:10.1097/OPX.0000000000000935

16. Scheiman M, Wick B. Clinical Management of Binocular Vision: Heterophoric, Accommodative and Eye Movement Disorders. 4th ed. Philadelphia, PA: Lippincott Williams & Wilkins; 2014.

17. Garzia RP, Richman JE, Nicholson SB, Gaines CS. A new visual-verbal saccade test: the Development Eye Movement test (DEM). J Am Optom Assoc. 1990;61(2):124-135.

18. Yeo BT, Krienen FM, Sepulcre J, et al. The organization of the human cerebral cortex estimated by intrinsic functional connectivity. J Neurophysiol. 2011;106(3):1125-1165. doi:10.1152/jn.00338.2011

19. Oishi K, Faria AV, Mori S. JHU-MNI-ss atlas. https://github.com/Jfortin1/EveTemplate. Accessed June 28, 2019.

20. Cox RW. AFNI: software for analysis and visualization of functional magnetic resonance neuroimages. Comput Biomed Res. 1996;29(3):162-173. doi:10.1006/cbmr.1996.0014

21. Nashner LM, Peters JF. Dynamic posturography in the diagnosis and management of dizziness and balance disorders. Neurol Clin. 1990;8(2):331-349. doi:10.1016/S0733-8619(18)30359-1

22. Wallace EJ, Mathias JL, Ward L. Diffusion tensor imaging changes following mild, moderate and severe adult traumatic brain injury: a meta-analysis. Brain Imaging Behav. 2018;12(6):1607-1621. doi:10.1007/s11682-018-9823-2

23. Shenton ME, Hamoda HM, Schneiderman JS, et al. A review of magnetic resonance imaging and diffusion tensor imaging findings in mild traumatic brain injury. Brain Imaging Behav. 2012;6(2):137-192. doi:10.1007/s11682-012-9156-5

24. Johnson VE, Stewart W, Smith DH. Axonal pathology in traumatic brain injury. Exp Neurol. 2013;246:35-43. doi:10.1016/j.expneurol.2012.01.013

25. Tang-Schomer MD, Patel AR, Baas PW, Smith DH. Mechanical breaking of microtubules in axons during dynamic stretch injury underlies delayed elasticity, microtubule disassembly, and axon degeneration. FASEB J. 2010;24(5):1401-1410. doi:10.1096/fj.09-142844